

Revisiting semileptonic B meson decays at next-to-next-to-leading order

Manuel Egner^a, Matteo Fael^b, Kay Schönwald^c, Matthias Steinhauser^a

(a) *Institut für Theoretische Teilchenphysik, Karlsruhe Institute of Technology (KIT),
Wolfgang-Gaede Straße 1, 76128 Karlsruhe, Germany*

(b) *Theoretical Physics Department, CERN, 1211 Geneva, Switzerland*

(c) *Physik-Institut, Universität Zürich, Winterthurerstrasse 190,
8057 Zürich, Switzerland*

Abstract

We compute next-to-next-to-leading order corrections to the semileptonic decay rate of B mesons for arbitrary values of the final-state quark mass. For the contribution with one massive quark in the final state, we extend the literature result and obtain analytic expressions in terms of iterated integrals. For the complete contribution, which also includes contributions with three massive quarks in the final state, we present a semi-analytic method, which leads to a precise approximation formula for the decay rate. Our results agree with the expansions available for $b \rightarrow c\ell\bar{\nu}_\ell$ and $b \rightarrow u\ell\bar{\nu}_\ell$ in the literature. The main emphasis of this paper is on the technical aspects of the calculation which are useful for a wider range of applications.

1 Introduction

The inclusive semileptonic $B \rightarrow X \ell \bar{\nu}_\ell$ decays, mediated by the charged-current transition $b \rightarrow q \ell \bar{\nu}_\ell$ with $q = u, c$, are standard probes of the CKM matrix elements V_{cb} and V_{ub} . The comparison between the experimental values of the branching ratios and their theoretical predictions obtained within the framework of the Heavy Quark Expansion has allowed the extraction of $|V_{cb}|$ with a 1.2% accuracy [1, 2] while for $|V_{ub}|$ it has reached about 5% [3].

The calculation of the decay rate in the free quark approximation, i.e. $\Gamma(b \rightarrow q \ell \bar{\nu}_\ell)$, constitutes one of the main theoretical ingredients for the extraction of the CKM elements. The decay rate is known in an exact form for arbitrary mass of the final state quark q only up to order α_s . At higher orders, results have been obtained only as asymptotic expansions either in the massless limit, with the expansion parameter $\rho = m_c/m_b \ll 1$, or the equal mass limit, with the expansion parameter $\delta = 1 - \rho = 1 - m_c/m_b \ll 1$.

At next-to-next-to-leading order (NNLO), expansions around $\rho \rightarrow 0$, which covers both $b \rightarrow u \ell \bar{\nu}_\ell$ and $b \rightarrow c \ell \bar{\nu}_\ell$, have been computed in Refs. [4, 5]. The asymptotic expansion in this limit is quite involved and it has not yet been extended to next-to-next-to-next-to-leading order (N³LO). At NNLO also the other limit $\delta \rightarrow 0$ was studied in Ref. [6] showing a much simpler asymptotic expansion (compared to the limit $\rho \rightarrow 0$) and a fast convergence of the series in δ even at the physical value of m_c . At N³LO an expansion around $m_c \simeq m_b$ has been performed in Ref. [7, 8] (see also Ref. [9] where a subset of diagrams have been cross-checked). Currently, the predictions for $b \rightarrow u$ at N³LO are based on expansions for $m_c \rightarrow m_b$ and a subsequent extrapolation to $m_c = 0$. This yields a sizable uncertainty of about 10%.

Recently, a semi-analytic method for the calculation of multi-loop Feynman integrals depending on one dimensionless parameter (and the dimension d) has been developed in Ref. [10]. It was applied successfully in QCD to the calculation of the fermionic part of the $\overline{\text{MS}}$ -pole mass relation at four loops and the massive form factors at three loops [11–13]. The “expand and match” method provides results well suited for fast numerical evaluation and sufficiently precise for phenomenological applications.

In this paper we reconsider the corrections of $O(\alpha_s^2)$ to the $b \rightarrow q \ell \bar{\nu}_\ell$ total rate, and revisit its calculation utilizing the method developed in [10]. The purpose is twofold. On the one hand, the application of the “expand and match” method to semileptonic decays serves as preparation for similar other calculations in B physics, such as the computation of non-leptonic decay rates at NNLO. It also provides cross checks of the known expansions around $\rho = 0$ and $\rho = 1$. On the other hand, we discuss for the first time the role of the rare decay $b \rightarrow c \bar{c} \ell \bar{\nu}_\ell$, which contains an additional $\bar{c}c$ pair in the final state. This decay channel was so far neglected in the expansions around the limit $m_c \simeq m_b$, both at NNLO and N³LO.

Let us further elaborate on the last point. At leading order and NLO, the possible real emission processes which contribute to the total semileptonic rate ($b \rightarrow c \ell \bar{\nu}_\ell$ and

$b \rightarrow cgl\bar{\nu}_\ell$) contain only one charm quark in the final state. Starting from NNLO, there is also a decay channel where three charm quarks appear in the final state (see, e.g., Figs. 1(a) and (e)).

For technical reasons (see below) the calculation for $m_c \simeq m_b$ includes only the contributions with one (massive) charm quark in the final state but neglects the contributions with three charm quarks. The latter is kinematically accessible only if $m_c < m_b/3$ and thus missing in the equal mass limit $m_c = m_b$. The contribution of the rare decay is very small, of the order of 10^{-7} , and so negligible for the physical value of the charm mass ($\rho \simeq 0.25$), without impact on the extraction of V_{cb} . However, in order to properly match the expansion around $\rho = 0$ and $\rho = 1$ it is crucial to correctly take into account the contribution of $b \rightarrow c\bar{c}l\bar{\nu}_\ell$.

The main results presented in this paper are the following:

- We compute analytic results for the NNLO correction in terms of iterated integrals for all contributions with one charm quark in the final state. We do not include contributions with three charm quarks since they would involve elliptic integrals originating, e.g., from four-loop sunrise diagrams with unequal masses.
- We construct a piece-wise defined function where the individual pieces are either Taylor or power-log expansions with (precise) numerical coefficients. This approximation contains all contributions, also those with three charm quarks in the final state. It reproduces the correct functional behaviour in the various kinematic limits at $\rho \rightarrow 0$ and $\rho \rightarrow 1$ but also at $\rho \rightarrow 1/3$.

The outline of this paper is as follows: In the next Section we introduce the notation and describe our analytic and numeric methods. Afterwards we discuss in Section 3 our results for the total decay rate of $b \rightarrow cl\bar{\nu}_\ell$ at NNLO. In particular, we present analytic results for the contributions with one and three charm quarks in the final state. We also discuss our approximation formulas and in particular their numerical accuracy. In Section 4 we present the calculation of the charm dependent contribution to the decay $b \rightarrow ul\bar{\nu}_\ell$, i.e. the two-loop diagrams with a closed charm loop insertion into the gluon propagator. Finally we summarize our findings in Section 5.

2 Methods

2.1 Notation

Let us now discuss the details of the calculation. We consider the decay of an on-shell bottom quark into a charged lepton (e, μ) assumed to be massless, a neutrino and any hadronic state X_c containing a charm quark:

$$b \rightarrow X_c l \bar{\nu}_\ell. \tag{1}$$

To compute the decay rate we apply the optical theorem and compute the imaginary part of the bottom quark two-point function. In the following we do not restrict ourselves to physical masses of $m_c \approx m_b/3$, rather we keep m_c generic. As we will see, for technical reasons the limit $m_c \rightarrow m_b$ is of high relevance. With $m_c \rightarrow 0$ we cover the case $b \rightarrow u\ell\bar{\nu}_\ell$. After specifying the QCD colour factors to QED, our results can also be applied to the muon and tau decays.

It is convenient to define the following variables:

$$\rho = \frac{m_c}{m_b}, \quad \delta = 1 - \frac{m_c}{m_b}.$$

We write the decay rate in the form

$$\Gamma(B \rightarrow X_c \ell \bar{\nu}) = \Gamma_0 \left[X_0 + C_F \sum_{n \geq 1} \left(\frac{\alpha_s}{\pi} \right)^n X_n \right] + \mathcal{O} \left(\frac{\Lambda_{\text{QCD}}^2}{m_b^2} \right), \quad (2)$$

where m_b and m_c are renormalized in the on-shell scheme,

$$\Gamma_0 = \frac{A_{\text{ew}} G_F^2 |V_{cb}|^2 m_b^5}{192 \pi^3}, \quad (3)$$

$C_F = 4/3$, $A_{\text{ew}} = 1.014$ is the leading electroweak correction [14], and $\alpha_s \equiv \alpha_s^{(5)}(\mu_s)$ with μ_s being the renormalization scale. The tree-level contribution is given by

$$X_0 = 1 - 8\rho^2 - 12\rho^4 \log(\rho^2) + 8\rho^6 - \rho^8. \quad (4)$$

The one- and two-loop results are available from Refs. [4–6, 15–19] and the three-loop correction X_3 has been computed in Ref. [7] (see also [9] for partial results). In the following we reconsider X_2 which is a function of the mass ratio m_c/m_b .

At leading order and NLO, the functions X_0 and X_1 come from Feynman diagrams with cuts only through one charm quark line. These diagrams develop an imaginary part for $0 \leq \rho < 1$. Starting at NNLO, there are also diagrams where three charm lines can be cut (see, e.g., Fig. 1(a) and (e)). They develop an additional discontinuity for $0 \leq \rho < 1/3$ which corresponds to the contribution of the rare decay $b \rightarrow c\bar{c}\ell\nu$.

In the following we present our calculation of X_2 which is divided in two steps. In a first step, we compute analytic results valid for arbitrary charm quark masses for the contribution to X_2 which does not contain three charm quarks in the final state. Later on, we present an approximation function for the complete contribution to X_2 , which consists of power-log expansions valid in certain m_c ranges.

2.2 General setup

We generate the amplitude with `qgraf` [20] and process the output with `tapir` [21]. Next we apply `exp` [22, 23] to map the individual diagrams to integral families. The actual

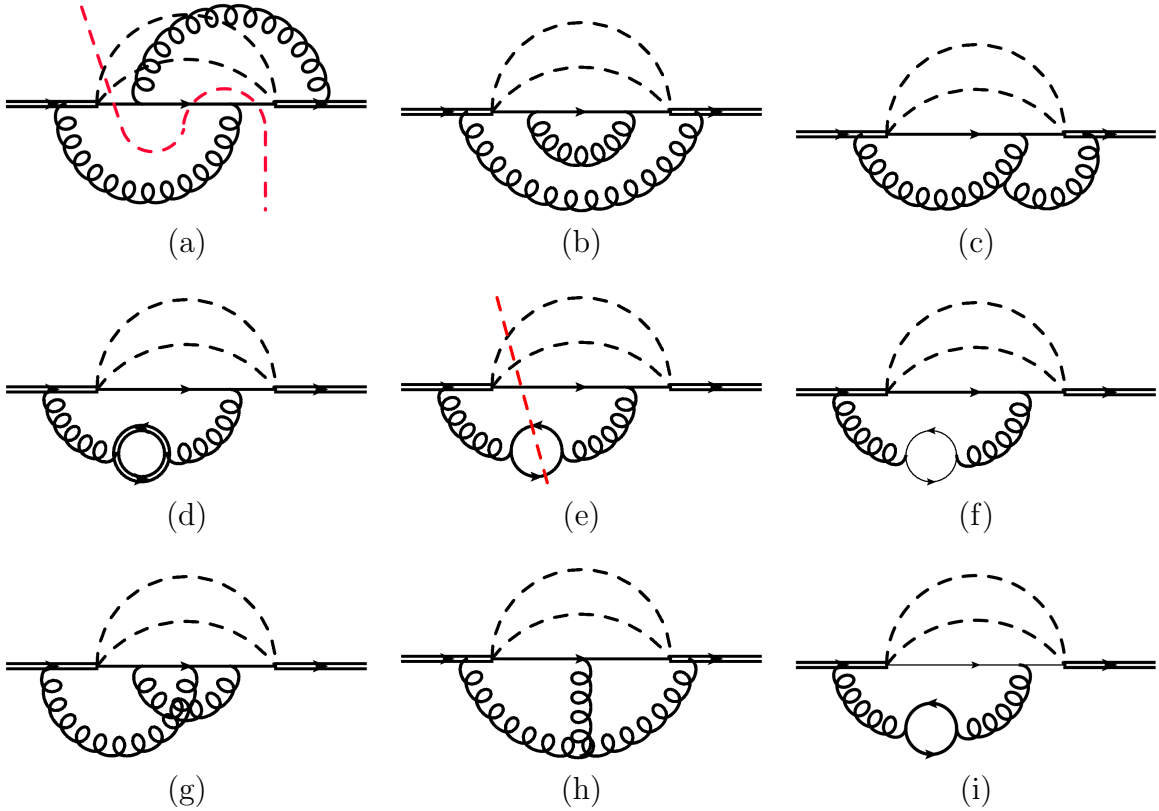


Figure 1: Sample diagrams contributing to the semileptonic B meson decays at NNLO. The dashed lines represent the charged lepton neutrino pair. Double lines denote bottom quarks, thick and thin lines denote charm and massless quarks, respectively. The red dashed lines shown for diagrams (a) and (e) indicate possible three-charm cuts.

computation is done with `FORM` [24]. At this step the auxiliary files generated by `tapir` are quite useful to express the amplitude for each diagram as a linear combination of scalar integrals.

They are reduced to master integrals with the use of `Kira` [25] in combination with `FireFly` [26] within each integral family. Furthermore, we apply `ImproveMasters` [27] in order to obtain for each integral family a basis such that the ϵ and ρ dependence in the denominators of each reduction table entry factorizes. Once all master integrals are identified we use again `Kira` to identify the symmetries across families and reduce the master integrals to a minimal set. In total we arrive at 129 four-loop master integrals. Samples of master integrals are shown in Fig. 2

Note that we do not exploit that it is in principle possible to integrate over the charged-lepton-neutrino loop in a first step since this cannot be done for the calculation of the non-leptonic B meson decays.

We perform the calculation for general QCD gauge parameter ξ . For most of the colour structures ξ drops out at the level of the bare amplitude. The remaining ξ dependence

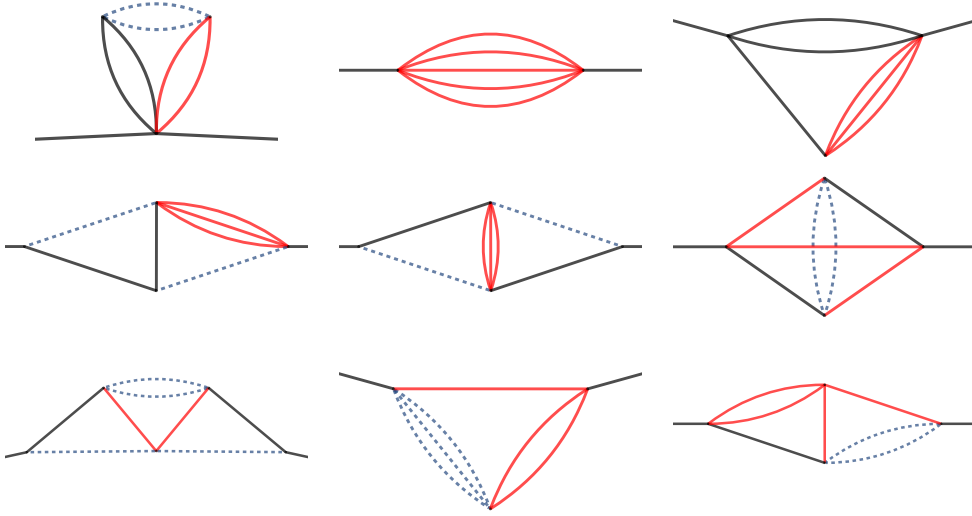


Figure 2: Samples of four-loop master integrals. Black and red solid lines represents massive propagator with mass m_b and m_c , respectively, while dashed lines are massless propagators.

cancel after the inclusion of the bottom mass counterterms.

A crucial input for the methods discussed in the next two subsections are the differential equations for the master integrals. They can easily be established using the reduction tables.

2.3 Analytic calculation

In this subsection we present our analytic calculation of the master integrals, in case we consider the contribution of cuts only through one charm quark. For the decay rate, we need in principle only the imaginary parts of the master integrals. As a consequence we can restrict ourself only to the masters which have a physical cut, i.e. where the propagator of neutrino, charged lepton and at least one charm propagator can be cut simultaneously. In Fig. 2, the master integrals in the first row do not have a physical cut, while those in the second and third row have an imaginary part.

The requirement of physical cuts reduces the number of master integrals from 129 to 108. We construct analytic solutions for the imaginary part of the master integrals with the help of the differential equations. We use boundary conditions from the limit $m_c \rightarrow m_b$ ($\rho \rightarrow 1$) where it is quite straightforward to compute the imaginary parts of the master integrals via an asymptotic expansion.

The crucial observation is that by fixing the boundary conditions at $m_c = m_b$ one calculates the contribution where only one charm line is cut. In fact, in this limit there is no possible discontinuity corresponding to a cut through three charm quarks, which appears

in Feynman integrals only for $0 \leq \rho < 1/3$ (i.e. $\delta > 2/3$). For example, the master integrals shown in the second row of Fig. 2 have a cut only through three charm lines (additionally to the lepton and neutrino), while those in the third row have a cut through one charm line. Note that for some of the masters, like the one on the right in the third row, both one-charm and three-charm cuts appear.

In order to incorporate the three-charm cut contribution, it would be necessary to compute a complicated asymptotic expansion around $\rho = 1/3$. Alternatively one can compute boundary conditions for both real and imaginary parts for $\rho > 1/3$ and solve the differential equations for the complete set of 129 master integrals. This would require the computation of four-loop on-shell integrals, which are to date not available in analytic form. The semi-analytic approach discussed in Section 2.4 covers this case. In the limit $m_c \rightarrow m_b$ only 95 out of the 129 master integrals have a cut through one charm line. Note that 13 master integrals have cuts only through 3 charm lines while the remaining 21 do not have an imaginary part.

Let us now discuss our analytic solution for the 95 masters with one charm cut. In a first step we transform the differential equation matrix in ϵ form [28, 29]. This is done using both `Libra` [30] and `Canonica` [31].

`Libra` is used to bring the matrix in block-diagonal form and afterwards we use `Canonica` to transform the whole system to ϵ form. This is done by first transforming the diagonal blocks and then the corresponding off-diagonal elements block by block, using the build-in functions of `Canonica`. This approach is successful for a subset of 91 master integrals. The remaining four integrals are at the top-level and can be decomposed into a 3×3 system and an uncoupled integral. We solve these integrals following the algorithm outlined in Ref. [32]. In practice this means that we decouple the coupled system with the package `OreSys` [33], which internally depends on `Sigma` [34], and solve the resulting higher order differential equation via factorization of the differential operator with the help of `HarmonicSums` [35]. In an independent calculation we have used this approach of solving the differential equation on the whole system and did not make use of the ϵ form of the first 91 master integrals. The results of both approaches are in complete agreement.

The ϵ form is conveniently obtained in the variables t which is defined via

$$\begin{aligned} \rho &= \frac{1-t^2}{1+t^2}, \\ t &= \frac{\sqrt{1-\rho}}{\sqrt{1+\rho}}. \end{aligned} \tag{5}$$

Then the solution can be expressed in terms of iterated integrals with the alphabet

$$\left\{ \frac{1}{1+t}, \frac{1}{t}, \frac{1}{1-t}, \frac{t}{1+t^2}, \frac{t^3}{1+t^4} \right\}. \tag{6}$$

For the computation of the boundary conditions we follow Refs. [7, 8, 36], where similar integrals have been considered. In [36, 37] the three-loop relation between the heavy

quark masses defined in the pole and kinetic scheme has been computed. The starting point in Refs. [7, 8] were five-loop integrals. A convenient choice of momentum routing and integration order led to a factorization, where at most three-loop integrals have to be solved. In the present calculation we deal with four-loop integrals and observe a similar factorization.

We apply the so-called “method of regions” [38] which in our case leads to a scaling of the loop momenta as either hard (h) or ultra-soft (us).¹ This leads to at most $2^4 = 16$ different regions for a given integral, however, not all of them contribute. For example, the region where all loop momenta are hard does not develop an imaginary part and can be discarded.

For the identification of the regions we use the package `asy.m` [39], which we apply to each master integral separately. As input it requires the list of propagators and the scalings of the masses and the external momenta. `asy.m` provides as output the scalings of the propagators for all non-vanishing regions. The comparison to the scalings which we obtain after identifying a unique routing of the loop momenta allows us to discard regions, which give no contribution. For the non-vanishing regions we can perform the expansions in the small parameter δ .

Note that in Refs. [7, 36], the program `asy.m` was only used as a cross check to make sure that all contributing regions were found. It was furthermore applied at the level of the amplitudes and not to master integrals. In the present calculation `asy.m` is used to discard regions which are zero before the expansion is done. Since we use it at the level of the master integrals, it is suitable to apply this procedure to each of the 95 master integrals separately.

Two of the four loop momenta have to be ultra-soft, namely the loop momentum of the charged-lepton-neutrino loop and the one which flows into the lepton loop. The remaining two loop momenta are either ultra-soft or hard.

The calculation of the Feynman integrals appearing from the asymptotic expansion closely follows Ref. [8] and can be summarized by the following steps. We consider separately the regions corresponding to the momentum scaling (h, h, us, us) , (h, us, us, us) and (us, us, us, us) . For each region we define new integral families that contain all propagators and numerators which arise after the expansion. We find symmetries across the new integral families with the program `LIMIT` [40], which is based on `LiteRed` [41]. In case there are linearly dependent propagators, we perform a partial fraction decomposition with `LIMIT` and minimize again the number of families. For each family, we perform a reduction to master integrals with `Kira` [25]. The master integral in the asymptotic expansion can be written in terms of Γ functions and, in one case, as a one-fold Mellin-Barnes integral. In particular, the master integrals with three or four ultra-soft loop momenta can be solved via recursive one-loop integration. In case we have two hard loop momenta, we observe a factorization into one- and two-loop integrals.

¹Following Ref. [38] we use the term ultra-soft instead of soft.

For convenience we provide the formulas for one-loop integrals used in the recursive integration (with $q^2 = 1$):

$$\begin{aligned}
I_1(p; n_1, n_2) &= \int \frac{d^d k_1}{(-k_1^2)^{n_1} (-(k_1 + p)^2)^{n_2}} \\
&= i\pi^{d/2} \frac{\Gamma(n_1 + n_2 - 2 + \epsilon) \Gamma(2 - n_2 - \epsilon) \Gamma(2 - n_1 - \epsilon)}{\Gamma(n_1) \Gamma(n_2) \Gamma(4 - n_1 - n_2 - 2\epsilon)} (-p^2)^{2-\epsilon+n_1+n_2}, \\
I_2(n_1, n_2) &= \int \frac{d^d k_1}{(-k_1^2)^{n_1} (-k_1^2 + 2k_1 \cdot q)^{n_2}} \\
&= i\pi^{d/2} \frac{\Gamma(n_1 + n_2 - 2 + \epsilon) \Gamma(4 - n_2 - 2n_1 - 2\epsilon)}{\Gamma(n_2) \Gamma(4 - n_1 - n_2 - 2\epsilon)}, \\
I_3(\delta; n_1, n_2, n_3) &= \int \frac{d^d k_1}{(-k_1^2)^{n_1} (-2q \cdot k_1)^{n_2} (-\delta - 2q \cdot k_1)^{n_3}} \\
&= i\pi^{d/2} (-\delta)^{4-2\epsilon-2n_1-n_2-n_3} \\
&\quad \frac{\Gamma(4 - 2\epsilon - 2n_1 - n_2) \Gamma(2 - \epsilon - n_1) \Gamma(2n_1 + n_2 + n_3 - 4 + 2\epsilon)}{\Gamma(n_1) \Gamma(n_3) \Gamma(4 - 2\epsilon - 2n_1)}.
\end{aligned}$$

In the hard regions, we used also the expression for the two-loop sunrise diagram with three equal masses:

$$\begin{aligned}
I_4(1, 1, 1) &= \int \frac{d^d k_1 d^d k_2}{(1 - (k_1 + k_2)^2) (1 - (k_1)^2) (1 - (k_2 + q)^2)} \\
&= (i\pi^{d/2})^2 \frac{1}{2\pi i} \int_{-i\infty}^{i\infty} dz \\
&\quad \frac{\Gamma(-z) \Gamma^2(1 - \epsilon - z) \Gamma(-1 + 2\epsilon + z) \Gamma(1 - \epsilon) \Gamma(2 - 2\epsilon - z)}{\Gamma(2 - 2\epsilon - 2z) \Gamma(3 - 3\epsilon - z) (-4)^{-1+2\epsilon+z}}. \quad (7)
\end{aligned}$$

We compute for each master integral the first two expansion coefficients for $\delta \rightarrow 0$. Note that not all δ coefficients are needed to fix the integration constants. There are diagonal blocks in the differential equation where several integrals are coupled. It is usually sufficient to choose one of the integrals and match it to its boundary condition including subleading δ terms. This allows us to fix all boundary conditions also for the remaining integrals in the block. Once all integration constants are fixed, we calculate from the analytic solution the δ expansion of all integrals. We use the coefficients which were not used as cross check. Altogether we have computed 192 coefficients in the δ expansion (two for each of the 95 master integrals) but we have used only 72 of them to fix the boundary constants.

Once all boundary conditions are fixed it is straightforward to integrate the differential equations up to the required order in ϵ . After inserting the master integrals into the amplitude, we expand in ϵ up to the constant term. The bare NNLO amplitude develops $1/\epsilon^2$ and $1/\epsilon$ poles which cancel against the counterterm contribution. Their transcendental

weight is one and two, respectively. In the ϵ^0 term we observe iterated integrals up to weight five even after choosing a minimal set of functions. The occurrence of weight-two expressions in the pole part is expected since this weight also appears in the analytic NLO result [42]. At first sight the weight-five functions in the finite three-loop term might be surprising. Note, however, that we start with four-loop integrals. Since the charged-lepton-neutrino loop is finite one can expect weight-six expressions from the remaining three-loop calculation. Since we compute the imaginary parts we finally end up with weight-five iterated integrals.

We refrain from presenting exact analytic results in the paper but refer to the supplementary material [43] where also the expressions for the imaginary part of the master integrals (one charm cut) can be found. In Section 3.1 we will present the analytic expansions of the decay rate in the limits $\rho \rightarrow 0$ and $\rho \rightarrow 1$.

2.4 Numeric calculation

As an alternative to the analytic approach described in the previous subsection, we discuss in the following the “expand and match” method introduced in Refs. [10, 12]. The starting point is the system of differential equations for the 129 master integrals obtained in Section 2.2. The basic idea of this method is as follows: We choose several points $\rho_0 \in [0, 1]$, make an ansatz for the expansion of the master integrals around $\rho = \rho_0$, insert the ansatz in the differential equations and solve the resulting system of linear equations for the coefficients in the ansatz in terms of a few initial values. The latter are determined by matching to known results.

The choice of expansion points ρ_0 should include all singular values of the differential equations that in our case are $\rho = 0, 1/3$ and 1 , where $\rho = 1/3$ corresponds to the three-charm threshold. Furthermore we add regular points to obtain higher precision approximation formulas. As expansion points we choose

$$\rho_0 \in \{0, 1/12, 1/6, 1/4, 1/3, 1/2, 1\}, \quad (8)$$

with $\rho_0 = 1/2$ as starting point. Note that the radius of convergence in general extends only up to the next singular point in the complex plane. As a consequence it is sufficient to choose only a few points above the threshold at $\rho = 1/3$. Below threshold more expansion points are needed in order to reach a good convergence. Furthermore we employ Möbius transformations (see Ref. [44]) to extend the radius of convergence of the series expansions into the direction of the farther singularity. Explicit ready-to-use formulas for our application can be found in Ref. [12].

The expansion around regular points is a simple Taylor expansion and thus we choose the following ansatz for the master integrals

$$I_i = \sum_{j=\epsilon_{\min}}^{\epsilon_{\max}} \sum_{n=0}^{n_{\max}} c_{i,j,n} \epsilon^j (\rho - \rho_0)^n, \quad (9)$$

where ϵ_{\min} is determined by the highest pole and ϵ_{\max} depends on the spurious poles in the amplitude in front of the respective master integral. For the expansion depth we typically choose $n_{\max} = 50$ which provides about ten or more significant digits in our final result.

For the singular points the ansatz has to be extended to allow for logarithmic terms. At $\rho_0 = 0$ we have

$$I_i = \sum_{j=\epsilon_{\min}}^{\epsilon_{\max}} \sum_{m=0}^{j+4} \sum_{n=0}^{n_{\max}} c_{i,j,m,n} \epsilon^j \rho^n \log^m(\rho). \quad (10)$$

At $\rho_0 = 1/3$ and $\rho_0 = 1$ our ansatz is

$$I_i = \sum_{j=\epsilon_{\min}}^{\epsilon_{\max}} \sum_{m=0}^{j+4} \sum_{n=n_{\min}}^{n_{\max}} c_{i,j,m,n} \epsilon^j (\rho - \rho_0)^n \log^m(\rho - \rho_0). \quad (11)$$

We choose $n_{\min} < 0$ to allow for potential negative powers. However, it turns out that only the coefficients for $n \geq 0$ are different from zero. In case our ansatz is insufficient the system of linear equations can either not be solved or only the trivial solution is possible.

The expansion around the three-particle threshold at $\rho = 1/3$ does not require the introduction of half-integer powers of $\rho - 1/3$, at variance with what is observed for two- and four-particle thresholds (e.g., see [11, 12]). In fact the production close to threshold of n particles of mass m behaves as [45, 46]

$$(s - (nm)^2)^{\frac{3n-5}{2}}, \quad (12)$$

where s is the squared energy available to the system. One observes that half-integer powers are arising only when an even number of particles are produced, while for an odd number the exponent is an integer.

As boundary condition for the “expand and match” procedure we choose $\rho_0 = 1/2$. We use **AMFlow** [47] to obtain numerical results for all master integrals (both real and imaginary part) with a precision of 80 digits and fix undetermined constants for the Taylor expansion around $\rho = 1/2$ (see Eq. (9)). Next we evaluate the master integrals at $\rho_0 = 0.4$ which serves as input for the expansion around $\rho_0 = 1/3$. We could proceed in a similar way towards $\rho = 1$. However, here we can use the analytic boundary conditions to produce a deep expansion in $1 - \rho$.

At $\rho_0 = 1/3$ we perform the matching at a value $\rho > 1/3$. Thus the logarithms in Eq. (11) are real-valued whereas the coefficients $c_{i,j,m,n}$ have both real and imaginary parts. After crossing the threshold to values of $\rho < 1/3$ the logarithms develop additional imaginary parts according to $\log(\rho - \rho_0) = \log(|\rho - \rho_0|) - i\pi$ which arise from the three-charm threshold. For the expansion around $\rho_0 = 1$ it is convenient to use the ansatz in Eq. (11) with $(\rho - \rho_0)$ replaced by $(\rho_0 - \rho)$ since we always have $\rho < \rho_0$ and thus we do not have to deal with spurious imaginary parts. In this way, we determine the coefficients of all expansions around the singular and regular points given in Eq. (8).

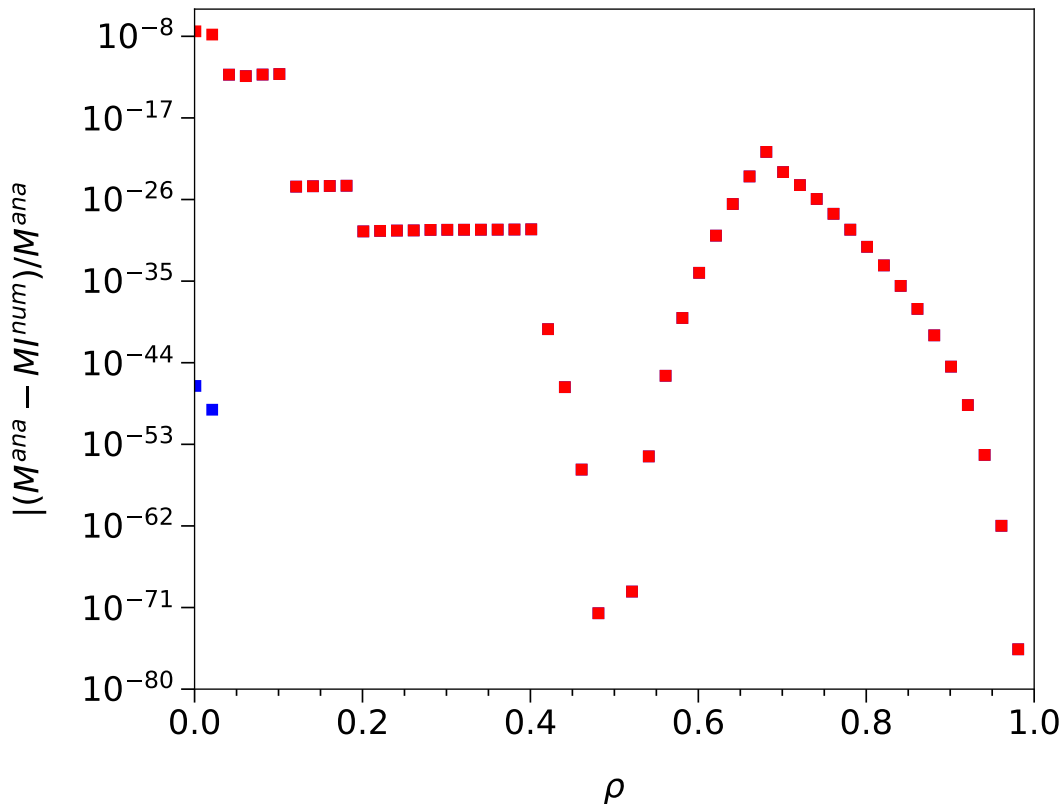


Figure 3: Relative difference between the semi-analytic approximation formula and the analytic result for the ϵ^0 term of the (imaginary part) of the fourth non-planar master integral shown in Fig. 4. The blue dots are obtained from the matching of the $\rho = 0$ expansion to boundary conditions computed at $\rho = 0.01$.

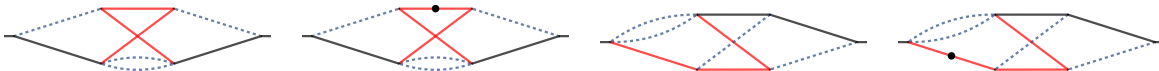


Figure 4: Master integrals with nine propagators which appear in the top sector of the differential equations. The dashed line denote massless propagators, black and red lines have mass m_b and m_c , respectively. Squared propagators are marked with a dot. The external lines are on-shell.

To check the precision of our results obtained with the “expand and match” approach, we compare them with the analytic expressions from Section 3.1 at $\rho > 1/3$. For the numerical evaluation of the iterated integrals we use `ginac` [48, 49]. As an example, we show in Fig. 3 the relative difference between the analytic and numerical result for the ϵ^0 coefficient of the fourth master integral with nine propagators in Fig. 4. The red dots in Fig. 3 show an agreement of more than 17 digits in the range $0.1 < \rho < 1$, with increasing precision when ρ approaches the value $1/2$ where the expansion was matched

to the numerical evaluation with `AMFlow`. Also the expansion around $\rho = 1$ manifests a good convergence when approaching $\rho = 1$ because this series expansion was matched to the analytic boundary condition calculated in the previous section. The lower-order ϵ terms and the master integrals in lower sectors show in general an even better agreement.

We observe a loss of precision (only 8 digits) when we approach the massless limit at $\rho = 0$ where several master integrals develop mass singularities. In principle the precision can be improved by including more (regular) expansion points between $\rho = 0$ and $\rho = 1/3$. Alternatively, we can recalculate the boundary condition with `AMFlow` at some point close to $\rho = 0$. For instance, the blue points shown in Fig. 4 correspond to the expansion around $\rho = 0$ matched to a numerical evaluation at $\rho = 1/100$. In this case, the precision is of more than 44 digits and thus shows that also in the massless case we can reach a good accuracy in the evaluation of the master integrals.

In principle it is possible to use `AMFlow` for the physical value of the charm quark mass. However, in that case we would lose the flexibility to vary the charm quark mass and to consider different mass schemes for the quarks. Furthermore, `AMFlow` cannot reproduce the power-log behaviour around the singular points. In fact, the evaluation with `AMFlow` at the threshold $\rho = 1/3$ or for $\rho = 0, 1$ yields only the hard parts in the asymptotic expansion around these two points. In our approach we obtain the same power-log expansions around the singular points as from an analytic calculation, where the expansion coefficients have a numerical accuracy of 10 and more.

3 Decay rates

We obtain the NNLO prediction to the decay rate after renormalizing the wave function of the external bottom quark in the on-shell scheme, the strong coupling constant α_s in the $\overline{\text{MS}}$ scheme with five active flavour, and m_c and m_b in the on-shell scheme. The on-shell masses can be converted to other short-distance mass schemes. We divide the coefficient X_2 appearing in the decay rate at order α_s^2 in two parts:

$$X_2(\rho) = X_2^{1c}(\rho) + X_2^{3c}(\rho), \quad (13)$$

which correspond to the contributions with one and three charm quarks in the final state.

3.1 Analytic result of contribution without cut through three charm lines

We use the results for the master integrals obtained in Section 2.3 to compute the decay rate at NNLO omitting the contributions involving three massive charm quarks in the final state, X_2^{1c} . For the physical values of the charm and bottom quark masses these contributions are negligible. However, they become sizable in case we approach the limit $m_c \rightarrow 0$ (see next subsection).

The exact expression for X_2^{1c} is too long to be printed here but can be downloaded from [43]. It contains in total 313 different iterated integrals constructed from the alphabet in Eq. (6) up to weight five. It can be numerically evaluated using `ginac` [48, 49].

With the help of `HarmonicSums` [35] we obtain analytic expansions around $\rho = 0$ and $\rho = 1$. For illustration we provide the first three expansion terms in both limits. Deeper expansion can be obtained from [43]. For the renormalization scale we choose $\mu = m_b$ and obtain

$$\begin{aligned}
X_2^{1c}|_{\rho \rightarrow 0} = & C_F \left\{ \frac{25775}{5184} - \frac{13339\pi^2}{2592} - \frac{101\zeta_3}{72} + \frac{17}{3}\pi^2 \log 2 + \frac{17\pi^4}{120} + \left(\frac{13}{8} - \frac{\pi^2}{4} + \zeta_3 \right) l_\rho \right. \\
& - \frac{5\pi^2}{3} \rho + \rho^2 \left[-\frac{45323}{162} + \frac{403\pi^2}{54} + \frac{599\zeta_3}{3} - \frac{20}{3}\pi^2 \log 2 + \frac{991\pi^4}{540} \right. \\
& \left. \left. - \left(\frac{290}{9} - \frac{4\pi^2}{3} \right) l_\rho^2 - \frac{14}{3} l_\rho^3 - \frac{2}{3} l_\rho^4 + \left(-\frac{6631}{54} + \frac{52\pi^2}{9} + 60\zeta_3 \right) l_\rho \right] \right\} \\
& + C_A \left\{ \frac{75623}{5184} - \frac{101\pi^2}{5184} - \frac{1111\zeta_3}{144} - \frac{17}{6}\pi^2 \log 2 + \frac{11\pi^4}{240} - \left(\frac{13}{16} - \frac{\pi^2}{8} + \frac{\zeta_3}{2} \right) l_\rho \right. \\
& + \frac{5\pi^2}{6} \rho + \rho^2 \left[-\frac{56207}{648} + \frac{7}{3} l_\rho^3 + \frac{1}{3} l_\rho^4 - \frac{745\pi^2}{108} - \frac{599\zeta_3}{6} + \frac{10}{3}\pi^2 \log 2 - \frac{331\pi^4}{1080} \right. \\
& \left. \left. - \left(\frac{5699}{108} + \frac{26\pi^2}{9} + 30\zeta_3 \right) l_\rho + \left(\frac{181}{9} - \frac{2\pi^2}{3} \right) l_\rho^2 \right] \right\} \\
& + T_F n_l \left[-\frac{1009}{288} + \frac{77\pi^2}{216} + \frac{8\zeta_3}{3} + \rho^2 \left(\frac{118}{3} - \frac{4\pi^2}{3} + \frac{52}{3} l_\rho - 8l_\rho^2 \right) \right] \\
& + T_F n_b \left[\frac{16987}{576} - \frac{85\pi^2}{216} - \frac{64\zeta_3}{3} + \rho^2 \left(-\frac{1198}{45} + \frac{8\pi^2}{3} \right) \right] \\
& + T_F n_c \left[\frac{20063}{5184} + \frac{61\pi^2}{216} + \frac{4\zeta_3}{3} + \frac{2}{9} l_\rho^3 + \frac{5}{3} l_\rho^2 + \left(\frac{415}{72} - \frac{\pi^2}{9} \right) l_\rho - \frac{13\pi^2}{8} \rho \right. \\
& \left. + \rho^2 \left(-\frac{1475}{162} + \frac{106\pi^2}{27} - \frac{184}{9} l_\rho - \frac{44}{3} l_\rho^2 \right) \right] + \dots, \tag{14}
\end{aligned}$$

$$\begin{aligned}
X_2^{1c}|_{\rho \rightarrow 1} = & C_F \left[\delta^5 \left(-\frac{46}{5} + \frac{32\pi^2}{5} - \frac{32}{5}\pi^2 \log 2 + \frac{48\zeta_3}{5} \right) + \delta^6 \left(\frac{69}{5} - \frac{48\pi^2}{5} + \frac{48}{5}\pi^2 \log 2 \right. \right. \\
& \left. \left. - \frac{72\zeta_3}{5} \right) + \delta^7 \left(\frac{39329}{3675} + \frac{3044\pi^2}{945} - \frac{496}{105}\pi^2 \log 2 + \frac{248\zeta_3}{35} - \frac{352}{105} l_{2\delta} \right) \right] \\
& + C_A \left\{ \delta^5 \left(-\frac{286}{15} - \frac{8\pi^2}{5} - \frac{24\zeta_3}{5} + \frac{16}{5}\pi^2 \log 2 \right) + \delta^6 \left(\frac{99}{5} + \frac{12\pi^2}{5} + \frac{36\zeta_3}{5} \right. \right. \\
& \left. \left. - \frac{24}{5}\pi^2 \log 2 \right) + \delta^7 \left[-\frac{99547507}{1157625} + \frac{62206\pi^2}{33075} + \frac{132\zeta_3}{35} + \frac{248}{105}\pi^2 \log 2 \right. \right. \\
& \left. \left. + \left(\frac{1333376}{33075} - \frac{256\pi^2}{315} \right) l_{2\delta} - \frac{1408}{315} l_{2\delta}^2 \right] \right\} + T_F n_l \left[\frac{56}{15} \delta^5 - \frac{12}{5} \delta^6 \right]
\end{aligned}$$

$$\begin{aligned}
& + \delta^7 \left(\frac{25577548}{1157625} - \frac{512\pi^2}{945} - \frac{417664}{33075} l_{2\delta} + \frac{512}{315} l_{2\delta}^2 \right) \Big] + T_F n_b \left[\delta^5 \left(\frac{184}{3} - \frac{32\pi^2}{5} \right) \right. \\
& + \delta^6 \left(-12 + \frac{8\pi^2}{5} \right) + \delta^7 \left(\frac{107444}{2835} - \frac{3848\pi^2}{945} \right) \Big] + T_F n_c \left[\delta^5 \left(\frac{184}{3} - \frac{32\pi^2}{5} \right) \right. \\
& \left. + \delta^6 \left(-\frac{828}{5} + \frac{88\pi^2}{5} \right) + \delta^7 \left(\frac{108580}{567} - \frac{18968\pi^2}{945} \right) \right] + \dots, \tag{15}
\end{aligned}$$

with $l_\rho = \log(\rho)$ and $l_{2\delta} = \log(2\delta)$. The ellipses stand for higher order terms in ρ and δ . For the expansion around $\rho = 1$, we obtain a power-log series starting with δ^5 . This is in agreement with the results from [6–8]. In the expansion around $\rho = 0$ we observe that for the color factors $C_F T_F n_l$ and $C_F T_F n_b$ the limit $\rho \rightarrow 0$ exists whereas the other three colour structures develop logarithmic divergences. The non-fermionic structures (C_F^2 and $C_F C_A$) contain linear logarithms in the leading expansion term. For the colour structure $C_F T_F n_c$ we have a cubic logarithm. These logarithms originate from the mass singularities. They cancel against the real radiation contribution contained in the three-charm contribution X_2^{3c} . At higher order in ρ also quartic logarithms start to appear; see, e.g., the colour factors C_F^2 and $C_F C_A$. We note that the coefficients of the odd expansion terms in ρ are simpler than those of the even terms.

The divergent behaviour of X_2^{1c} for $\rho \rightarrow 0$ is due to the mass singularities for massless charm quarks which are present since not all possible cuts are considered. In the complete result as computed in Refs. [4, 5] the limit $\rho \rightarrow 0$ exists. We can subtract the expansion in Eq. (14) from the result computed in Refs. [4, 5] to obtain analytic expressions for the contribution from three-charm cuts. We obtain

$$\begin{aligned}
X_2^{3c}|_{\rho \rightarrow 0} = & C_F \left\{ -\frac{409}{576} - \frac{349\pi^2}{288} - \frac{115\zeta_3}{24} + \frac{19}{6}\pi^2 \log 2 - \frac{7\pi^4}{144} - \left(\frac{13}{8} - \frac{\pi^2}{4} + \zeta_3 \right) l_\rho + \frac{5\pi^2}{3} \rho \right. \\
& + \rho^2 \left[\frac{12083}{648} - \frac{103\pi^2}{36} - \frac{341\zeta_3}{3} - \frac{4}{3}\pi^2 \log 2 - \frac{29\pi^4}{18} + \left(\frac{961}{54} - \frac{52\pi^2}{9} - 60\zeta_3 \right) l_\rho \right. \\
& \left. \left. - \left(\frac{34}{9} + \frac{4\pi^2}{3} \right) l_\rho^2 + \frac{14}{3} l_\rho^3 + \frac{2}{3} l_\rho^4 \right] \right\} + C_A \left\{ \frac{409}{1152} + \frac{349\pi^2}{576} - \frac{19}{12}\pi^2 \log 2 \right. \\
& + \frac{115\zeta_3}{48} + \frac{7\pi^4}{288} - \frac{5\pi^2}{6} \rho + \left(\frac{13}{16} - \frac{\pi^2}{8} + \frac{\zeta_3}{2} \right) l_\rho + \rho^2 \left[-\frac{12083}{1296} + \frac{103\pi^2}{72} + \frac{341\zeta_3}{6} \right. \\
& \left. + \frac{2}{3}\pi^2 \log 2 + \frac{29\pi^4}{36} - \left(\frac{961}{108} - \frac{26\pi^2}{9} - 30\zeta_3 \right) l_\rho + \left(\frac{17}{9} + \frac{2\pi^2}{3} \right) l_\rho^2 - \frac{7}{3} l_\rho^3 - \frac{1}{3} l_\rho^4 \right] \right\} \\
& + T_F n_c \left[-\frac{38225}{5184} + \frac{2\pi^2}{27} + \frac{4\zeta_3}{3} + \left(-\frac{415}{72} + \frac{\pi^2}{9} \right) l_\rho - \frac{5}{3} l_\rho^2 - \frac{2}{9} l_\rho^3 + \frac{3\pi^2}{8} \rho \right. \\
& \left. + \rho^2 \left(\frac{9305}{162} + \frac{38\pi^2}{27} + \frac{340}{9} l_\rho + \frac{20}{3} l_\rho^2 \right) \right] + \dots \tag{16}
\end{aligned}$$

A deeper expansion is again available from [43]. After specifying the QCD colour factors to QED, the result in Eq. (16) yields the LO branching ratio also for the rare muon decay $\mu \rightarrow e(e^+e^-)\nu_\mu\bar{\nu}_e$ in an analytic form. We find perfect agreement with the numerical results for the branching ratio in Refs. [50, 51].

3.2 Numeric results of complete contributions

The “expand and match” approach described in Section 2.4 provides results for the whole ρ range as (power-log) expansions around values ρ_i with numerical coefficients. Each expansion is used in the respective convergence region.

There are a number of checks of our results which we describe in the following. A strong check of the individual master integrals is provided by the comparison to results obtained with `AMFlow` at various values for ρ . The numerical results we obtain from `AMFlow` are compared to the values we obtain from the power-log expansion of the masters. Looking at the relative difference, we observe that in the region between $\rho = 1$ and the threshold at $\rho = 1/3$ the accuracy for the Taylor expansions is of the order of 10^{-35} to 10^{-40} . When we match to the expansion around threshold, we loose some precision (because of the more complicated expansion) and observe for the Taylor expansions a relative difference of the order of 10^{-15} to 10^{-20} in the region between the threshold and $\rho = 0$. After matching to the power-log expansion around $\rho = 0$ we loose again some precision. Nevertheless we can reproduce the coefficients of the analytic expansion from Refs. [4, 5] to 8 or more digits, see also below.

The bare NNLO expression contains spurious ϵ poles which are introduced during the integration-by-parts reduction. After inserting results for the master integrals we observe poles up to sixth order. Since the counterterm contributions provide at most $1/\epsilon^2$ poles the higher poles have to cancel in the bare NNLO result. In the worst case we observe a pole cancellation of order 10^{-15} for certain $1/\epsilon^3$ poles while for the higher poles the cancellation is much better.

We obtain the renormalized decay rate by adding the counterterm in analytic form. The cancellation of the poles in ϵ provides a check on the numerical precision of our result. To quantify the accuracy we introduce the quantity

$$\delta(X_2|_{\epsilon^i}) = \left| \frac{X_2^{\text{bare}}|_{\epsilon^i} + X_2^{\text{CT}}|_{\epsilon^i}}{X_2^{\text{CT}}|_{\epsilon^i}} \right|. \quad (17)$$

In Fig. 5 we show $\delta(X_2|_{\epsilon^{-2}})$ and $\delta(X_2|_{\epsilon^{-1}})$ for $0 \leq \rho \leq 1$. Close to the starting point at $\rho = 1/2$ both the linear and quadratic poles cancel with more than 70 digits and then accuracy deteriorates when the distance from $\rho = 1/2$ increases. Here the accuracy is limited by the truncation of the expansion around $\rho = 1/2$.

When moving towards $\rho = 0$ the accuracy slightly deteriorates. Close to $\rho = 0$ we observe still a precision of about 8 digits. The blue and green points in Fig. 5 shows the precision in the $1/\epsilon^2$ and $1/\epsilon$ poles in case we use the $\rho = 0$ expansion matched to the `AMFlow` evaluation at $\rho = 1/100$.

To check the numerical accuracy of our approximation we compare for $\rho > 1/3$ against analytic results presented in the previous subsection. In Fig. 6 we show for the decay rate the relative difference between the analytic result and the semi-analytic approximation. For the “expand and match” approach we have used boundary conditions obtained with

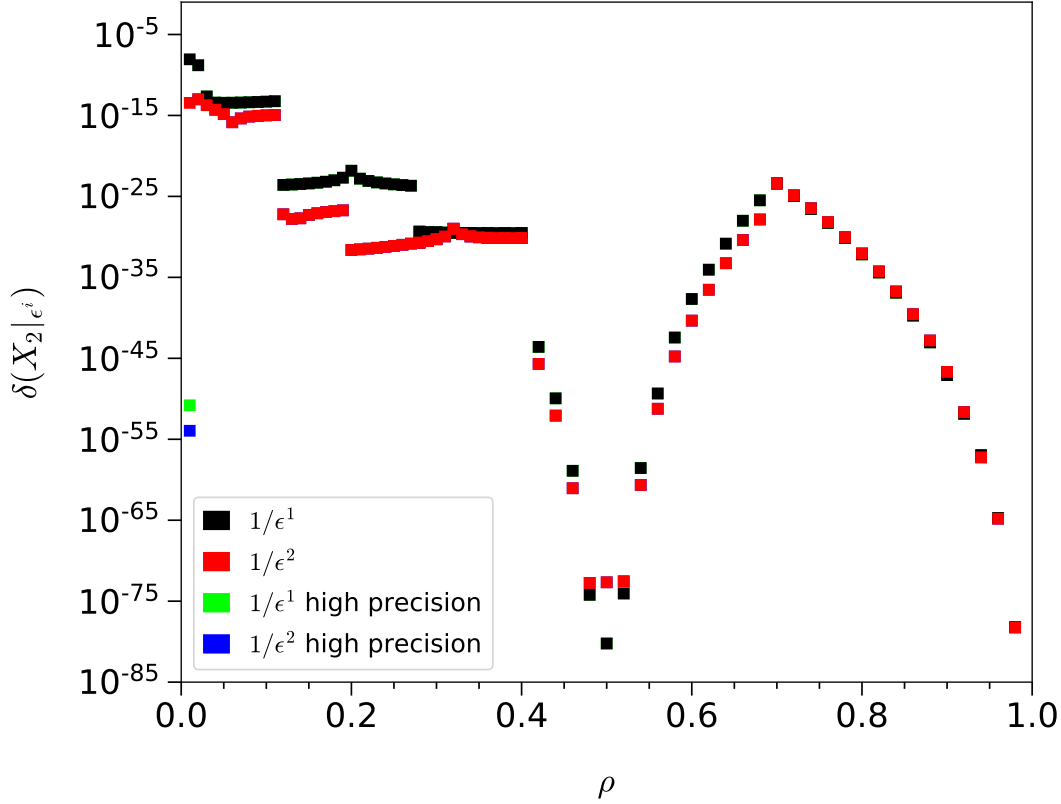


Figure 5: Relative precision for the cancellation of the $1/\epsilon$ poles according to Eq. (17). All colour factors have been set to their numerical values.

AMFlow for $\rho = 1/2$. Over the whole range of ρ we observe an agreement of at least 19 digits.

A further strong check of our result comes from the comparison of our expansion for $\rho \rightarrow 0$ to the results of Refs. [4, 5]. Using boundary conditions from $\rho = 1/2$ and transporting the solution of the master integrals at $\rho = 0$, we can reproduce the analytic coefficients of the asymptotic expansion at $\rho = 0$ with 10 digits for $n = 0$ which decreases to 8 for $n = 5$.

Alternatively we can also use the $\rho = 0$ expansion matched at $\rho = 1/100$. In this case we reproduce the analytic coefficients [4, 5] with more than 50 digits. Note that in our approach it is possible to obtain without any effort 50 expansion terms for $\rho \rightarrow 0$.

In Fig. 7 we show the NNLO contribution X_2 to the decay rate. The complete result is shown in red. For comparison we also show the contribution which only contains cuts through one charm quark (black curve, see Section 2.3). The strong $\log^3 \rho$ behaviour for small values of ρ is clearly visible, however, only very close to $\rho = 0$. The blue curve represents the contribution with three charm quarks in the final state. It has the same

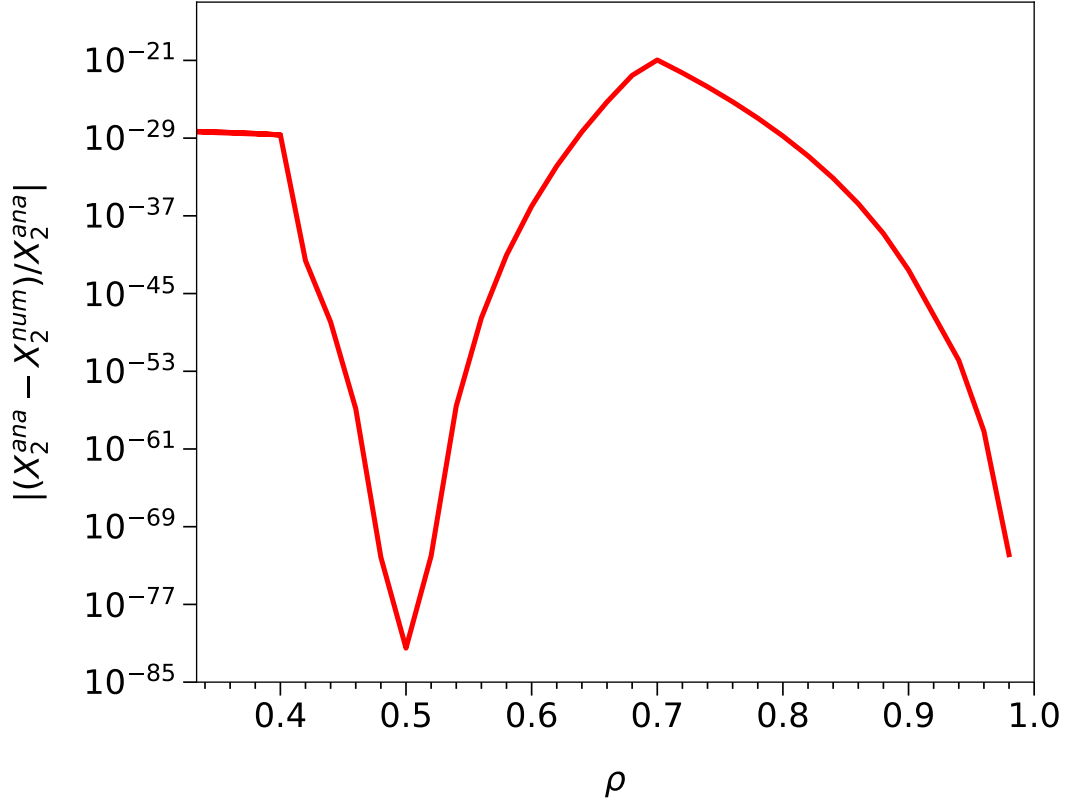


Figure 6: Relative difference between the semi-analytic approximation and the analytic results for the NNLO contribution X_2 to the decay rate. For the comparison we have set all colour factors to their numerical values. We consider the region $1/3 < \rho < 1$ since for $\rho < 1/3$ there are three-charm contributions which are not contained in the analytic result.

logarithmic behaviour with an opposite sign such that after adding it to the black curve one obtains the complete NNLO corrections with a smooth limit for $\rho \rightarrow 0$.

Finally we note that the three charm contribution to the decay rate is extremely suppressed at the physical value of the charm and bottom masses and therefore irrelevant for the current accuracy in the extraction of $|V_{cb}|$. At $\rho = 0.2$ we have $X_2^{3c} = 4 \times 10^{-5}$ which yields $\text{Br}(b \rightarrow c\bar{c}l\bar{\nu}_\ell) = 4 \times 10^{-8}$.

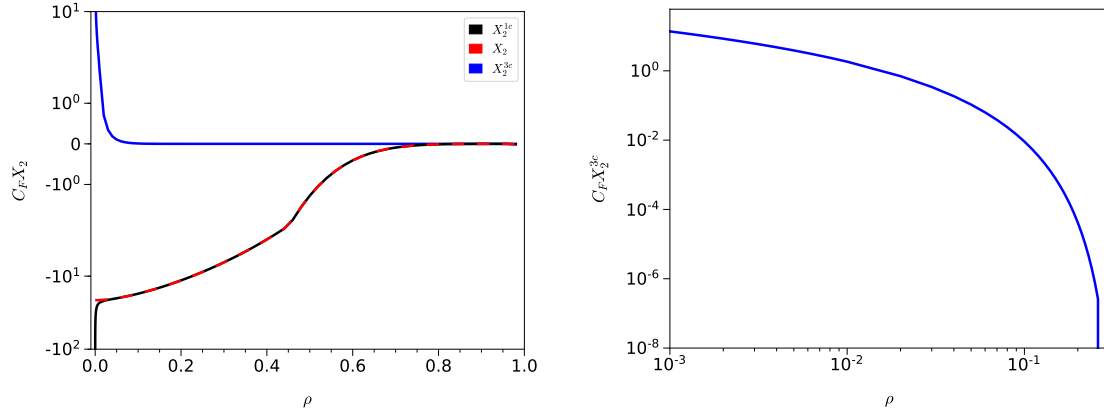


Figure 7: The complete result (dashed, red) is compared with the individual contributions which only contain cuts through one (black) or three charm quark lines (blue), respectively. The right panel shows the three-charm contribution is a double logarithmic plot.

4 Charm quark contribution in $b \rightarrow u$ decay rate at NNLO

In this Section we compute the charm quark mass dependence to $b \rightarrow u\ell\bar{\nu}_\ell$ at NNLO which arises from diagrams as the one shown in Fig. 1(i). In analogy to Eq. (2) we write

$$\Gamma(B \rightarrow X_u \ell \bar{\nu}) = \Gamma_0 \left[1 + \left(\frac{\alpha_s}{\pi} \right)^2 C_F T_F X_2^C + \dots \right] + \mathcal{O} \left(\frac{\Lambda_{\text{QCD}}^2}{m_b^2} \right), \quad (18)$$

with $T_F = 1/2$. The ellipses stand for charm quark-independent contributions. In the following we discuss the results for X_2^C .

In total, there are four Feynman diagrams. After integration-by-parts reduction, we find 16 master integrals. For the computation of the master integrals we again apply the “expand and match” approach and use **AMFlow** in order to obtain the boundary conditions. In contrast to $b \rightarrow c\ell\bar{\nu}_\ell$ we have cuts through two charm quarks and thus the threshold is located at $\rho = 1/2$ instead of $\rho = 1/3$. This means the singular points are $\rho = 0$ and $1/2$. For the expansion around $\rho_0 = 0$ we can use the ansatz given in Eqs. (10). For $\rho_0 = 1/2$ a new ansatz is necessary since we expect the occurrence of square roots according to Eq. (12). We therefore have

$$I_i = \sum_{j=\epsilon_{\min}}^{\epsilon_{\max}} \sum_{m=0}^{j+4} \sum_{n=n_{\min}}^{n_{\max}} c_{i,j,m,n} \epsilon^j (\sqrt{\rho - \rho_0})^n \log^m (\sqrt{\rho - \rho_0}), \quad (19)$$

where $\rho_0 = 1/2$. Again we allow for negative values of n_{\min} . However, the solution for the differential equations requires $n \geq 0$. We note that the additional imaginary parts induced by the two particle threshold are now generated by both the square roots and the logarithms.

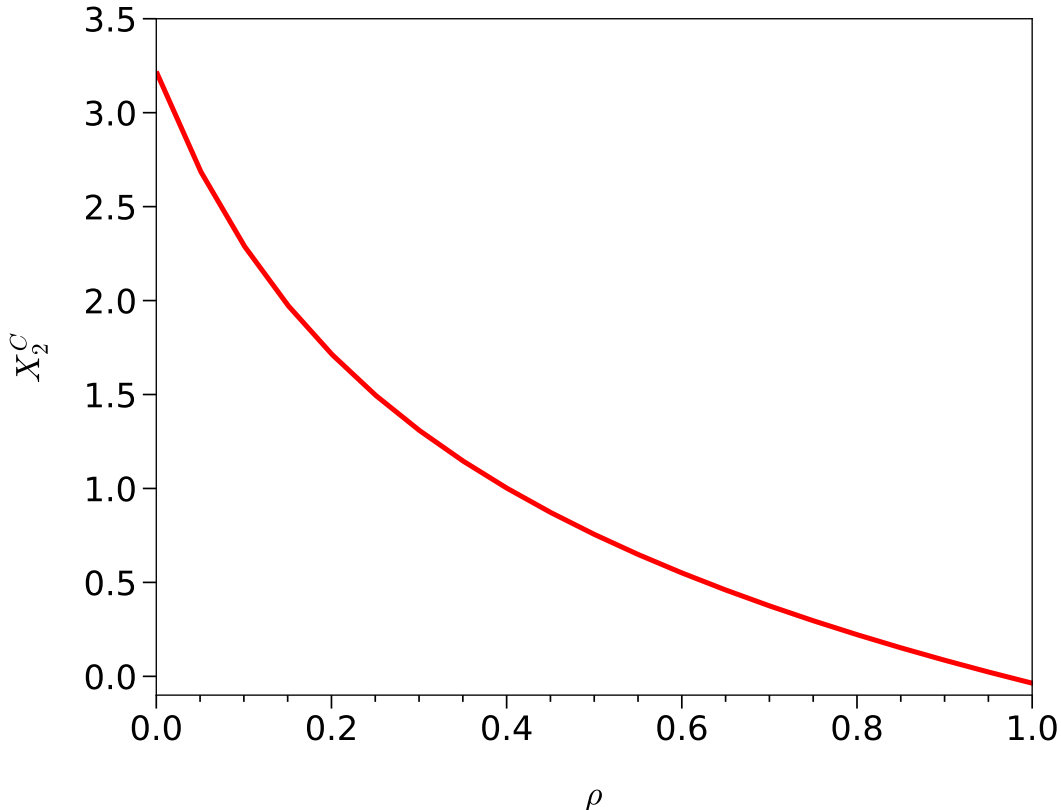


Figure 8: X_2^C as a function of ρ .

Finite results for the decay rate are obtained after renormalizing the bottom wave function in the on-shell and α_s in the $\overline{\text{MS}}$ scheme. Results for this contribution are given in Eq. (A6) of Ref. [5] in an expansion for $\rho \rightarrow 0$ up to ρ^7 . We use numerical boundary conditions at $\delta' = 0.1$ ($\rho \approx 0.95$) and apply repeatedly the “expand and match” approach to go over the two-charm threshold and to obtain a semi-analytic expansion around $\rho = 0$ (including 50 expansion terms). We can compare the individual coefficients of $\rho^n \log^k(\rho)$ to the analytic results of Ref. [5] and find agreement to at least 9 significant digits. For $\rho = 1$ we can compare to the n_b term of the $b \rightarrow c$ decay which is obtained from Eq. (14) after setting $\rho = 0$. We observe agreement at the level of 10^{-30} . Similarly, for $\rho = 0$ we compare to the n_l term of Eq. (14) and find agreement within 9 digits. This shows again the power of our approach. Let us again stress that our numerical precision can be systematically improved by choosing more expansion points ρ_0 , deeper expansion depths or an appropriately chosen value for ρ to compute the boundary terms. In Fig. 8 we show X_2^C as a function of ρ .

5 Conclusions and outlook

In this work we reconsider the NNLO corrections to the semileptonic decay of a bottom quark to a charm quark. In the literature expansions are available [4–6] which are sufficient for phenomenological studies. The aim of this paper is to provide semi-analytic power-log expansions which are valid for $0 \leq \rho = m_c/m_b \leq 1$. Furthermore, we provide analytic results for the subset of Feynman diagrams which have contributions with one charm quark in the final state.

For the semi-analytic calculation we use the “expand and match” [10, 12] method to transport information about the master integrals at a given starting point $\rho = \rho_0$ to any value of ρ . It uses the differential equations in combination with an appropriate ansatz to construct a semi-analytic approximation formula which is composed of power-log expansions valid in certain sub-intervals of $\rho \in [0, 1]$. To obtain the initial values of the master integrals we use `AMFlow` [47]. Our approach is able to properly take into account singular behaviours of the exact (unknown) function. In our case this concerns the expansions around $\rho = 0, 1/3$ and 1. We also compute the charm dependent contributions to $b \rightarrow u\ell\bar{\nu}_\ell$ at NNLO. Here the singular points are at $\rho = 0$ and $1/2$.

The method developed in this paper serves as preparation for the computation of non-leptonic decay rates at NNLO. In these cases the techniques used for the semileptonic decays to obtain expansions are either not applicable or technically quite challenging. On the other hand it is straightforward to extend the semi-analytic approach of the present paper.

We want to remark that the method described in this paper can be applied at N³LO if the reduction to master integrals is possible and the system of differential equations can be established. However, it seems that at the moment the latter is a serious bottleneck.

Acknowledgements

We thank F. Lange for the help with `Kira`, V. Shtabovenko for the help with `Canonica` and K. Melnikov for useful discussions. This research was supported by the Deutsche Forschungsgemeinschaft (DFG, German Research Foundation) under grant 396021762 — TRR 257 “Particle Physics Phenomenology after the Higgs Discovery” and has received funding from the European Research Council (ERC) under the European Union’s Horizon 2020 research and innovation programme grant agreement 101019620 (ERC Advanced Grant TOPUP). The work of M.F. is supported by the European Union’s Horizon 2020 research and innovation program under the Marie Skłodowska-Curie grant agreement No. 101065445 – PHOBIDE.

References

- [1] M. Bordone, B. Capdevila and P. Gambino, Phys. Lett. B **822** (2021), 136679 [arXiv:2107.00604 [hep-ph]].
- [2] F. Bernlochner, M. Fael, K. Olschewsky, E. Persson, R. van Tonder, K. K. Vos and M. Welsch, JHEP **10** (2022), 068 [arXiv:2205.10274 [hep-ph]].
- [3] Y. S. Amhis *et al.* [Heavy Flavor Averaging Group and HFLAV], Phys. Rev. D **107** (2023) no.5, 052008 [arXiv:2206.07501 [hep-ex]].
- [4] A. Pak and A. Czarnecki, Phys. Rev. Lett. **100** (2008), 241807 [arXiv:0803.0960 [hep-ph]].
- [5] A. Pak and A. Czarnecki, Phys. Rev. D **78** (2008), 114015 [arXiv:0808.3509 [hep-ph]].
- [6] M. Dowling, J. H. Piclum and A. Czarnecki, Phys. Rev. D **78** (2008), 074024 [arXiv:0810.0543 [hep-ph]].
- [7] M. Fael, K. Schönwald and M. Steinhauser, Phys. Rev. D **104** (2021) no.1, 016003 [arXiv:2011.13654 [hep-ph]].
- [8] M. Fael, K. Schönwald and M. Steinhauser, JHEP **08** (2022), 039 [arXiv:2205.03410 [hep-ph]].
- [9] M. Czakon, A. Czarnecki and M. Dowling, Phys. Rev. D **103** (2021), L111301 [arXiv:2104.05804 [hep-ph]].
- [10] M. Fael, F. Lange, K. Schönwald and M. Steinhauser, JHEP **09** (2021), 152 [arXiv:2106.05296 [hep-ph]].
- [11] M. Fael, F. Lange, K. Schönwald and M. Steinhauser, Phys. Rev. Lett. **128** (2022) no.17, 172003 doi:10.1103/PhysRevLett.128.172003 [arXiv:2202.05276 [hep-ph]].
- [12] M. Fael, F. Lange, K. Schönwald and M. Steinhauser, Phys. Rev. D **106** (2022) no.3, 034029 doi:10.1103/PhysRevD.106.034029 [arXiv:2207.00027 [hep-ph]].
- [13] M. Fael, F. Lange, K. Schönwald and M. Steinhauser, Phys. Rev. D **107** (2023) no.9, 094017 [arXiv:2302.00693 [hep-ph]].
- [14] A. Sirlin, Nucl. Phys. B **196** (1982), 83-92
- [15] M. Trott, Phys. Rev. D **70** (2004), 073003 [arXiv:hep-ph/0402120 [hep-ph]].
- [16] V. Aquila, P. Gambino, G. Ridolfi and N. Uraltsev, Nucl. Phys. B **719** (2005), 77-102 [arXiv:hep-ph/0503083 [hep-ph]].
- [17] K. Melnikov, Phys. Lett. B **666** (2008), 336-339 [arXiv:0803.0951 [hep-ph]].

- [18] S. Biswas and K. Melnikov, *JHEP* **02** (2010), 089 [arXiv:0911.4142 [hep-ph]].
- [19] P. Gambino, *JHEP* **09** (2011), 055 [arXiv:1107.3100 [hep-ph]].
- [20] P. Nogueira, *J. Comput. Phys.* **105** (1993), 279-289;
<http://cfif.ist.utl.pt/~paulo/qgraf.html>.
- [21] M. Gerlach, F. Herren and M. Lang, *Comput. Phys. Commun.* **282** (2023), 108544 [arXiv:2201.05618 [hep-ph]].
- [22] R. Harlander, T. Seidensticker and M. Steinhauser, *Phys. Lett. B* **426** (1998) 125 [hep-ph/9712228].
- [23] T. Seidensticker, hep-ph/9905298.
- [24] B. Ruijl, T. Ueda and J. Vermaseren, [arXiv:1707.06453 [hep-ph]].
- [25] J. Klappert, F. Lange, P. Maierhöfer and J. Usovitsch, *Comput. Phys. Commun.* **266** (2021), 108024 [arXiv:2008.06494 [hep-ph]].
- [26] J. Klappert, S. Y. Klein and F. Lange, *Comput. Phys. Commun.* **264** (2021), 107968 [arXiv:2004.01463 [cs.MS]].
- [27] A. V. Smirnov and V. A. Smirnov, *Nucl. Phys. B* **960** (2020), 115213 [arXiv:2002.08042 [hep-ph]].
- [28] J. M. Henn, *Phys. Rev. Lett.* **110** (2013), 251601 [arXiv:1304.1806 [hep-th]].
- [29] R. N. Lee, *JHEP* **04** (2015), 108 [arXiv:1411.0911 [hep-ph]].
- [30] R. N. Lee, *Comput. Phys. Commun.* **267** (2021), 108058 [arXiv:2012.00279 [hep-ph]].
- [31] C. Meyer, *Comput. Phys. Commun.* **222** (2018), 295-312 [arXiv:1705.06252 [hep-ph]].
- [32] J. Ablinger, J. Blümlein, P. Marquard, N. Rana and C. Schneider, *Nucl. Phys. B* **939** (2019), 253-291 [arXiv:1810.12261 [hep-ph]].
- [33] S. Gerhold, *Uncoupling systems of linear Ore operator equations*, Diploma Thesis, RISC, J. Kepler University, Linz, 2002.
- [34] C. Schneider, *Sém. Lothar. Combin.* **56** (2007) 1, article B56b; C. Schneider, in: *Computer Algebra in Quantum Field Theory: Integration, Summation and Special Functions Texts and Monographs in Symbolic Computation* eds. C. Schneider and J. Blümlein (Springer, Wien, 2013) 325 arXiv:1304.4134 [cs.SC].

- [35] J. A. M. Vermaseren, *Int. J. Mod. Phys. A* **14** (1999), 2037-2076 [arXiv:hep-ph/9806280 [hep-ph]]; J. Blümlein, *Comput. Phys. Commun.* **180** (2009), 2218-2249 [arXiv:0901.3106 [hep-ph]]; J. Ablinger, Diploma Thesis, J. Kepler University Linz, 2009, arXiv:1011.1176 [math-ph]; J. Ablinger, J. Blümlein and C. Schneider, *J. Math. Phys.* **52** (2011) 102301 [arXiv:1105.6063 [math-ph]]; J. Ablinger, J. Blümlein and C. Schneider, *J. Math. Phys.* **54** (2013), 082301 [arXiv:1302.0378 [math-ph]]; J. Ablinger, Ph.D. Thesis, J. Kepler University Linz, 2012, arXiv:1305.0687 [math-ph]; J. Ablinger, J. Blümlein and C. Schneider, *J. Phys. Conf. Ser.* **523** (2014), 012060 [arXiv:1310.5645 [math-ph]]; J. Ablinger, J. Blümlein, C. G. Raab and C. Schneider, *J. Math. Phys.* **55** (2014), 112301 [arXiv:1407.1822 [hep-th]]; J. Ablinger, *PoS LL2014* (2014), 019 [arXiv:1407.6180 [cs.SC]]; J. Ablinger, [arXiv:1606.02845 [cs.SC]]; J. Ablinger, *PoS RADCOR2017* (2017), 069 [arXiv:1801.01039 [cs.SC]]; J. Ablinger, *PoS LL2018* (2018), 063; J. Ablinger, [arXiv:1902.11001 [math.CO]].
- [36] M. Fael, K. Schönwald and M. Steinhauser, *Phys. Rev. D* **103** (2021) no.1, 014005 [arXiv:2011.11655 [hep-ph]].
- [37] M. Fael, K. Schönwald and M. Steinhauser, *Phys. Rev. Lett.* **125** (2020) no.5, 052003 [arXiv:2005.06487 [hep-ph]].
- [38] M. Beneke and V. A. Smirnov, *Nucl. Phys. B* **522** (1998), 321-344 [arXiv:hep-ph/9711391 [hep-ph]].
- [39] A. Pak and A. Smirnov, *Eur. Phys. J. C* **71** (2011), 1626 [arXiv:1011.4863 [hep-ph]].
- [40] F. Herren, “Precision Calculations for Higgs Boson Physics at the LHC - Four-Loop Corrections to Gluon-Fusion Processes and Higgs Boson Pair-Production at NNLO,” PhD thesis, 2020, KIT.
- [41] R. N. Lee, *J. Phys. Conf. Ser.* **523** (2014), 012059 [arXiv:1310.1145 [hep-ph]].
- [42] Y. Nir, *Phys. Lett. B* **221** (1989), 184-190
- [43] <https://www.ttp.kit.edu/preprints/2023/ttp23-030/>.
- [44] R. N. Lee, A. V. Smirnov and V. A. Smirnov, *JHEP* **03** (2018), 008 [arXiv:1709.07525 [hep-ph]].
- [45] A. I. Davydychev and V. A. Smirnov, *Nucl. Phys. B* **554** (1999), 391-414 [arXiv:hep-ph/9903328 [hep-ph]].
- [46] K. Melnikov, private communication.
- [47] X. Liu and Y.-Q. Ma, *Comput. Phys. Commun.* **283** (2023), 108565 [arXiv:2201.11669 [hep-ph]].
- [48] C. W. Bauer, A. Frink and R. Kreckel, *J. Symb. Comput.* **33** (2000) 1 [cs/0004015 [cs-sc]].

- [49] J. Vollinga and S. Weinzierl, *Comput. Phys. Commun.* **167** (2005) 177 [[hep-ph/0410259](#)].
- [50] M. Fael and C. Greub, *JHEP* **01** (2017), 084 doi:[10.1007/JHEP01\(2017\)084](#)
- [51] G. M. Pruna, A. Signer and Y. Ulrich, *Phys. Lett. B* **765** (2017), 280-284 [[arXiv:1611.03617 \[hep-ph\]](#)].